

ORIGINAL ARTICLE

Multicenter evaluation of parametric response mapping as an indicator of bronchiolitis obliterans syndrome after hematopoietic stem cell transplantation

Guang-Shing Cheng¹ | Katherine E. Selwa² | Charles Hatt³ | Sundaresh Ram⁴ | Aleksa B. Fortuna⁴ | Margaret Guerriero⁵ | Ben Himelhoch⁶ | Daniel McAree⁷ | Timothy C. Hoffman² | Joseph Brisson⁸ | Ryan Nazareno⁸ | Kiernan Bloye⁸ | Timothy D. Johnson⁹ | Mats Remberger¹⁰ | Jonas Mattsson¹⁰ | Dharshan Vummid⁴ | Ella E. Kazerooni⁴ | Vibha N. Lama¹¹ | Stefanie Galban⁴ | Michael Boeckh¹ | Gregory A. Yanik⁸ | Craig J. Galban⁴ 

¹Clinical Research Division, Fred Hutchinson Cancer Research Center, Seattle, Washington

²University of Michigan Medical School, Ann Arbor, Michigan

³Imbio, LLC Minneapolis, Minneapolis, Minnesota

⁴Department of Radiology, Michigan Medicine, Ann Arbor, Michigan

⁵Seattle Cancer Care Alliance, Seattle, Washington

⁶Michigan State University College of Human Medicine, Lansing, Michigan

⁷Pediatrics, University of Michigan, Ann Arbor, Michigan

⁸Blood and Marrow Transplant Program, Michigan Medicine, Ann Arbor, Michigan

⁹Department of Biostatistics, University of Michigan, School of Public Health, Ann Arbor, Michigan

¹⁰Department of Oncology-Pathology, Karolinska University Hospital, Stockholm, Sweden

¹¹Division of Pulmonary and Critical Care Medicine, Michigan Medicine, Ann Arbor, Michigan

Correspondence

Craig J. Galban

Email: cgalban@med.umich.edu

Parametric response mapping (PRM) is a novel computed tomography (CT) technology that has shown potential for assessment of bronchiolitis obliterans syndrome (BOS) after hematopoietic stem cell transplantation (HCT). The primary aim of this study was to evaluate whether variations in image acquisition under real-world conditions affect the PRM measurements of clinically diagnosed BOS. CT scans were obtained retrospectively from 72 HCT recipients with BOS and graft-versus-host disease from Fred Hutchinson Cancer Research Center, Karolinska Institute, and the University of Michigan. Whole lung volumetric scans were performed at inspiration and expiration using site-specific acquisition and reconstruction protocols. PRM and pulmonary function measurements were assessed. Patients with moderately severe BOS at diagnosis (median forced expiratory volume at 1 second [FEV1] 53.5% predicted) had similar characteristics between sites. Variations in site-specific CT acquisition protocols had a negligible effect on the PRM-derived small airways disease (SAD), that is, BOS measurements. PRM-derived SAD was found to correlate with FEV1% predicted and FEV1/ forced vital capacity ($R = -0.236$, $P = .046$; and $R = -0.689$, $P < .0001$, respectively), which suggests that elevated levels in the PRM measurements are primarily affected by BOS airflow obstruction and not CT scan acquisition parameters. Based on these results, PRM may be applied broadly for post-HCT diagnosis and monitoring of BOS.

Abbreviations: BOS, bronchiolitis obliterans syndrome; COPD, chronic obstructive pulmonary disease; CT, computed tomography; Emph, emphysematous lung parenchyma; FEV1, forced expiratory volume at 1 second; FH, Fred Hutchinson Cancer Research Center; fSAD, functional small airways disease; FVC, forced vital capacity; HCT, hematopoietic stem cell transplantation; HU, Hounsfield unit; KI, Karolinska University Hospital; Norm, normal lung parenchyma; PD, parenchymal disease; PRM, parametric response mapping; SAD, small airways disease; TLC, total lung capacity; UM, University of Michigan.

Gregory A. Yanik and Craig J. Galban share senior authorship.

Funding information

National Institute of Health, Grant/Award Number: P30CA015704, P30CA046592, R01HL139690, R35CA197701, R44HL118837 and R44HL140894

KEY WORDS

biomarker, bone marrow/hematopoietic stem cell transplantation, bronchiolitis obliterans syndrome (BOS), clinical research/practice, diagnostic techniques and imaging: computed tomography, translational research/ science

1 | INTRODUCTION

Bronchiolitis obliterans syndrome (BOS) is a chronic obstructive airway disease associated with chronic graft-versus-host disease (GVHD) that occurs in 5%-12% of allogeneic hematopoietic cell transplant (allo-HCT) recipients.¹⁻⁷ The disorder is characterized by progressive fibro-obliteration of terminal bronchioles, with resultant air trapping, progressive dyspnea, recurrent pulmonary infections, and an overall decrease in quality of life as well as increased nonrelapse mortality.⁸ Most patients do not come to clinical attention until symptoms arise, at which point lung function decline is already severe and irreversible. The ability to identify and treat patients earlier in their clinical course is critical to reducing the morbidity and mortality associated with this condition.⁹ The National Institutes of Health (NIH) consensus guidelines for the diagnosis of chronic GVHD, however, do not allow for recognition of early BOS, atypical phenotypes of airflow obstruction, or restrictive lung disease (RLD).¹⁰ Novel imaging biomarkers that can serve as an adjunct to standard spirometry are needed to improve the assessment of early disease.

Parametric response mapping (PRM) is a voxel-based approach for analyzing high-resolution X-ray computed tomography (HRCT) images that provides detailed information on disease phenotype otherwise unattainable by conventional CT-based quantitative measures.¹¹ Using inspiratory and expiratory HRCT scans, PRM allows for the quantification of small airway disease (SAD) that contributes to airflow obstruction. PRM has been developed as a quantitative imaging biomarker for the assessment of obstructive lung disease in both chronic obstructive pulmonary disease (COPD)¹¹ and BOS postlung allografts.^{12,13} The potential utility of PRM for assessing SAD due to BOS after HCT has been recently examined in a single center cohort of BOS after allo-HCT with and without the presence of infection. Although a specific PRM signature was capable of identifying BOS even in the presence of interstitial pneumonitis in HCT recipients from a single site,¹⁴ variability in CT acquisition may affect the ability to apply PRM CT scans acquired at multiple sites. The primary aim of the current study was to evaluate whether variations in image acquisition under real-world conditions affect the PRM measurements of clinically diagnosed BOS. In addition, we describe features of PRM that may distinguish between phenotypes of BOS and RLD potentially related to chronic GVHD.

2 | MATERIALS AND METHODS**2.1 | Subjects**

Allo-HCT recipients diagnosed with BOS were accrued as part of a multicenter retrospective observational study. Participating sites

included the Karolinska University Hospital (KI), Fred Hutchinson Cancer Research Center (FH), and University of Michigan (UM). Any patients with a clinical diagnosis of BOS between the years 2000 and 2015, with a high-resolution chest CT and a pulmonary function test within 28 days of BOS diagnosis, were included. Additional subjects with chronic GVHD and restrictive lung disease were also included for an exploratory analysis. The study was approved by the Institutional Review Boards (IRBs) at all participating sites. In addition, all patients had signed an IRB-approved informed consent for data collection and analysis.

Pulmonary function tests (PFTs) were obtained as per clinical care guidelines of each respective institution. Forced expiratory volume in 1 second percent predicted (FEV1%), forced vital capacity percent predicted (FVC%), FEV1/FVC ratio, and total lung capacity percent predicted (TLC%) were based on accepted reference values that reflected the population served by each institution (Table 1). The clinical diagnosis of BOS was established on a site-by-site basis through clinical care. These criteria included modified NIH consensus criteria: FEV1 < 75% predicted, signs of obstructive airway disease (FEV1/FVC ratio < 0.7, residual volume [RV] > 120% predicted, or evidence of air trapping on high-resolution CT), the absence of infection, and the presence of chronic GVHD in another organ.¹⁵ Additional criteria for BOS diagnosis included

TABLE 1 Subject characteristics at each site

	KI	FH	UM
Number of cases (N)	12	48	12
Age (y)	44.7 (15.9)	56.2 (15)	59.3 (12)
Sex (M/F)	7/5	29/19	8/4
Height (cm)	67 (12.8)	74.8 (20.8)	70.9 (16.9)
Weight (kg)	169.7 (8)	169.6 (10.9)	172.5 (5.6)
Diagnosed Post-Tx (y)	1.96 (2.32)	3.04 (2.17)	1.33 (0.71) [†]
FEV1 (% predicted)	49.5 (21.8)	54.0 (25.8)	61.0 (22.5)
FVC (% predicted)	65.5 (23.0)	81.5(23.5) [*]	76.0 (30.3)
FEV1/FVC	0.72 (0.29)	0.55 (0.25) [†]	0.55 (0.16; N = 10) ^{P = .06}
TLC (% predicted)	84.0 (31.3)	96.0 (20.0)	112.0 (33.0; N = 5)

Note: Data are presented as the mean (standard deviation), except for FEV1, FVC, FEV1/FVC, and TLC presented as median (interquartile range; number of cases is adjusted). Significant pairwise differences are indicated as * for Site KI and FH and † for Site FH and UM. Continuous variables were tested using a univariable ANOVA controlling for multiple comparisons using the Bonferroni post hoc test. Sex was tested using a χ^2 test.

Abbreviations: FEV1, forced expiratory volume at 1 s; FVC, forced vital capacity; TLC, total lung capacity; Tx, transplantation.

decline in FEV1 and FVC with normal TLC, in the absence of infection or other causes for airflow decline,¹⁶ as well as those with mixed obstructive and restrictive ventilatory impairment based on obstruction by FEV1/FVC ratio < 0.7 or elevated RV with a concomitant decline in TLC. A small subset of patients with restrictive physiology in the presence of chronic GVHD were also included (N = 3 RLD only and N = 8 BOS/RLD).

2.2 | CT acquisition

CT examinations were performed using site-specific acquisition and reconstruction protocols (Table S1). For all sites, paired CT scans were acquired at full inspiration (TLC) and relaxed expiration (functional residual capacity). Quantitative CT data were presented in Hounsfield units (HU), where stability of CT measurement for each scanner was monitored based on site-specific protocols. For reference, air, water, and blood attenuation values should be -1000, 0, and 50 HU, respectively.¹⁷

2.3 | Parametric response mappings

PRM was applied to all paired CT scans as previously described.^{11,14} Briefly, lungs from both paired CT scans were segmented from the thoracic cavity using an in-house algorithm written in Matlab (The MathWorks, Inc). The whole-lung inspiratory CT scan was spatially aligned to the expiratory CT scan using Elastix, an open source image registration algorithm.^{18,19} This process allows the paired images to share the same geometric space, where each voxel, the smallest unit of volume in a 3-dimensional image data set, consists of HU values at inspiration and expiration. To mitigate the effects of noise on the PRM analysis, a 3 × 3 median filter was applied to all slices in the paired CT scans. Finally, all voxels bounded between -1000 and -250 HU on both paired CT scans were classified based on a scheme of 3 predetermined thresholds as previously described.¹⁴ Voxels with values greater than or equal to -950 HU and less than -810 HU at inspiration and greater than or equal to -856 HU at expiration were classified normal (PRM^{Norm}, green voxels), greater than or equal to -950 HU and less than -810 HU at inspiration and less than -856 HU at expiration were functional small airways disease (fSAD) (PRM^{fSAD}, yellow voxels), less than -950 HU at inspiration and less than -856 HU at expiration were emphysema (PRM^{Emph}, red voxels), and greater than or equal to -810 HU at inspiration were parenchymal disease (PD) (PRM^{PD}, purple voxels). The relative lung volumes, calculated as the sum of all voxels within a class normalized to the sum of all voxels within the expiratory lungs multiplied by 100, were used as global measures.

2.4 | Statistical analysis

All data values are presented as the mean ± standard deviation, unless specified otherwise. Site comparisons were determined for all

variables, that is, mean and standard deviation of HU values, patient characteristics, and PFT and PRM measures. Analysis of variance, controlling for multiple comparisons using a Bonferroni post hoc test, and χ^2 tests were used to assess site differences in continuous and categorical variables, respectively. Paired Student's *t* test was used to assess differences in the mean HU of ambient and tracheal air measured on inspiration and expiration CT scans from each site. PRM measures were correlated with PFT outcomes using a non-parametric Spearman rho correlation. Finally, univariable and multivariable analyses were performed to determine the contributions of PRM^{fSAD} and PRM^{PD} to FEV1%, FVC%, FEV1/FVC, and TLC% using an ANOVA and ANCOVA controlling for site and BMI, respectively. Results were considered statistically significant at the 2-sided 5% comparison-wise significance level ($P < .05$). All statistical computations were performed with a statistical software package (IBM SPSS Statistics, v. 21). Box and whiskers plots, generated using GraphPad Prism 7 (San Diego, CA), are presented as the 25th and 75th percentiles for the lower and upper box, respectively, median value for the line in the box, 5th and 95th percentiles for lower and upper whiskers, respectively, and markers as outliers.

3 | RESULTS

3.1 | Subject and site characteristics

In total, 72 patients were enrolled, including 12 patients from KI, 48 patients from FH, and 12 patients from UM (Table 1). The KI cohort included 6 subjects with BOS, including 3 with mixed obstruction/restriction and 3 patients with GVHD who had restriction on PFT. The FH cohort were all clinically identified as BOS with airflow obstruction, including 5 patients with mixed obstruction/restriction. The UM cohort were identified as BOS and all had obstruction. Negligible differences were observed between patient characteristics. FH patients were diagnosed up to 1.08 and 1.71 ($P = .04$) years later than patients diagnosed at KI and UM, respectively. The median FEV1% predicted at diagnosis were 49.5% (interquartile range [IQR] = 21.8%), 54.9% (IQR = 25.8%), and 61.0% (IQR = 22.5%) for KI, FH, and UM, respectively. In addition, there were no site differences in TLC. Significantly higher median FVC% and lower median FEV1/FVC were observed in the FH cohort (81.5%, IQR 23.5 and 0.55, IQR 0.25, respectively) when compared to KI (65.5%, IQR 23.0 and 0.72, IQR 0.29, respectively). Significant variations in the acquisition and reconstruction of chest CT scans between and within sites were observed. Representative CT slices acquired at full inspiration and expiration demonstrate the effect of imaging protocol on image quality and noise (Figure 1A,B). Details regarding the technical aspects of the CT reconstructions and analyses are provided in the Supplemental section. Presented in Figure 1C,D are examples of PRM images with corresponding scatter plots of individual lung voxels. All subjects had elevated levels of fSAD (the relative volume of lung with voxels greater than or equal to -950 HU and less than -810 HU at inspiration and less than -856 at expiration) compared to what

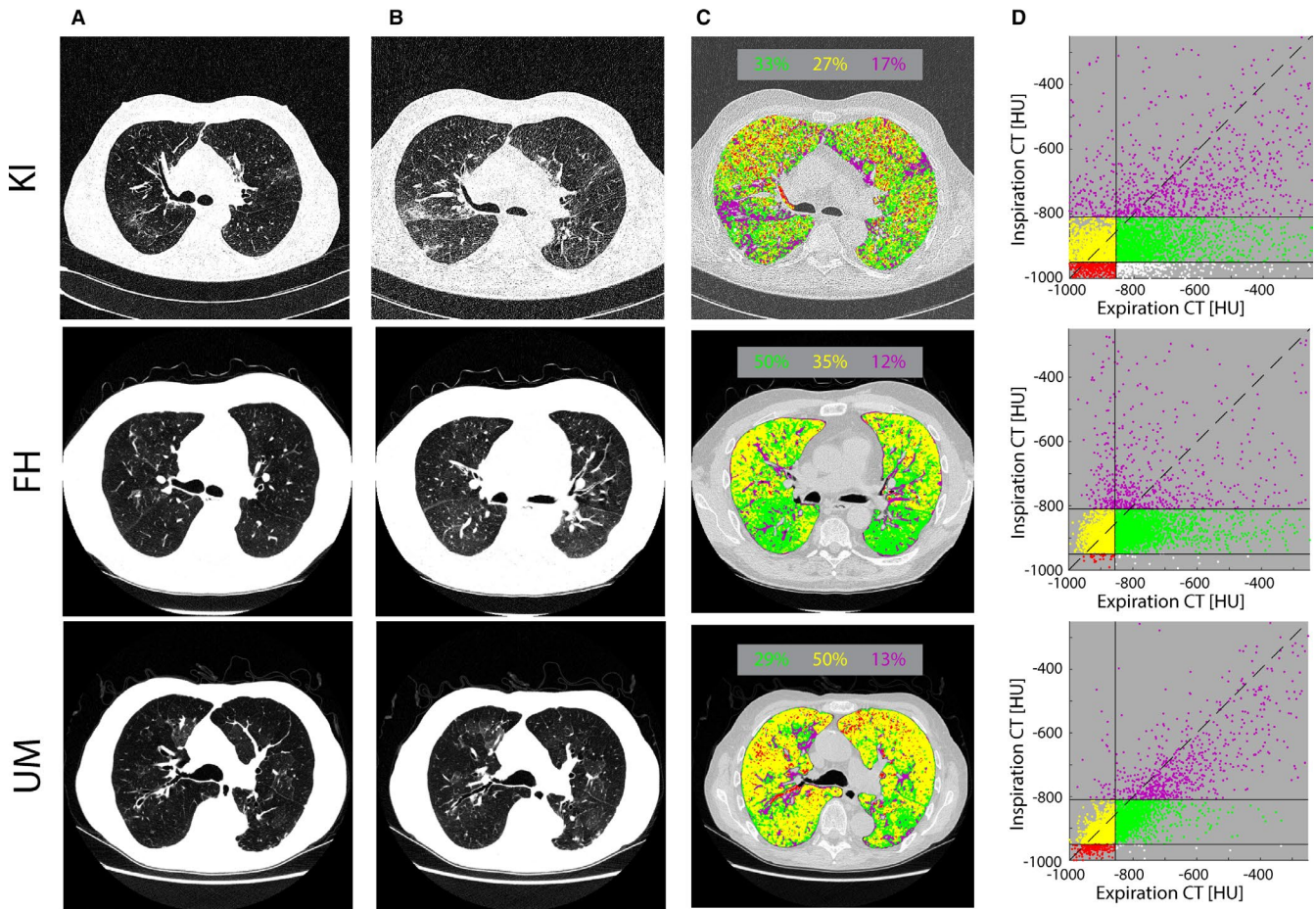


FIGURE 1 Effect of site-specific imaging protocol on PRM. Presented are representative axial slices from CT scans acquired at (A) inspiration, (B) expiration, (C) PRM overlay, and (D) corresponding PRM scatter plot from an individual case at each participating site. Peak voltage, tube current, slice thickness, and slice number/arrangement varied between cases. For the inspiration, CT scan protocol parameters were: (KI) 120 kVp, 249 mA, 0.6 mm, 708/contiguous; (FH) 120 kVp, 410 mA, 1.25 mm, 122/contiguous; and (UM) 120 kVp, 372 mA, 1.25 mm, 521/contiguous. For the expiration, CT scan protocol parameters were: (KI) 120 kVp, 66 mA, 0.6 mm, 635/contiguous; (FH) 120 kVp, 180 mA, 1.25 mm, 12/incremental; and (UM) 120 kVp, 376 mA, 1.25 mm, 502/contiguous. PRM-derived values over the whole lung are provided within an insert above each PRM image. The green value and markers represent normal parenchyma, yellow value and markers represent fSAD (ie, BOS), and magenta value and markers represent parenchymal disease. Age, sex, and percent predicted values of FEV1 and FVC for each case were: (KI) 63 y, male, 40%, and 62%; (FH) 57 y, male, 71%, and 94%; and (UM) 68 y, male, 44%, and 71%. BOS, bronchiolitis obliterans syndrome; CT, computed tomography; FEV1, forced expiratory volume at 1 s; FH, Fred Hutchinson Cancer Research Center; fSAD, functional small airways disease; FVC, forced vital capacity; KI, Karolinska University Hospital; PRM, parametric response mapping; UM, University of Michigan

is observed from a healthy population (PRM-derived fSAD = 5%–15%^{12–14}). On close examination of Figure 1C, PRM data for the KI case showed less spatial consolidation (ie, noisier) of individual classifications as compared to the representative cases at FH and UM. Figure 2 shows the relative volume of PRM-derived Normal (Norm), fSAD, and PD for all subjects separated by site. Although the relative volumes of normal and diseased parenchyma were found to differ between sites, these results were not significant. FH was found to have higher, yet nonsignificant, values in fSAD compared to KI and UM. PRM-derived fSAD and PD from all 3 sites were found to be elevated compared to healthy smokers ($8.4 \pm 1\%$ for fSAD and $11 \pm 2\%$ for PD) reported in our previous work.¹⁴ PRM-derived emphysema measurements (data not shown) were found to be significantly different between KI ($4.0\% \pm 5.3\%$) and FH ($0.9\% \pm 1.4\%$; $P = .001$) and

UM ($1.4\% \pm 1.7\%$; $P = .04$). Although the differences were significant, these values were small relative to PRM-derived fSAD and PD. All CT scans were radiographically confirmed by a trained thoracic radiologist (DV) to be absent of emphysema, which suggests that site differences in the relative volume of emphysema are most likely attributed to the higher HU scatter observed in the KI scans (Figure 1 and Figure S1).

3.2 | Effect of disease severity and phenotype on PRM

Analyses were performed to identify the contribution of disease severity and phenotype, as defined by PFT, on PRM measurements.

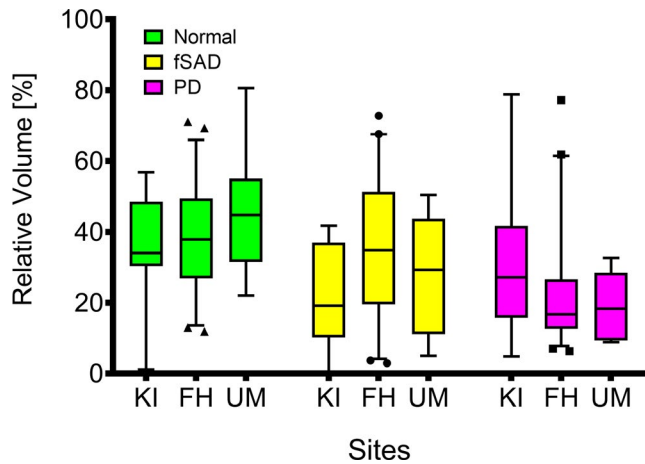


FIGURE 2 Evaluation of the site differences in PRM measurements. Box and whisker plots are presented for the relative volume of PRM-derived measurements from paired CT scans acquired at each site. The line within the box, the box extremes, and whiskers represent the median value, 25%ile and 75%ile, and 5%ile and 95%ile, respectively. Markers represent outliers beyond 5%ile and 95%ile. Site differences in variables were tested using a univariable ANOVA controlling for multiple comparisons using the Bonferonni post hoc test. Significance was assessed at a P value of .05. No significant differences were observed between sites for the presented measurements. CT, computed tomography; FH, Fred Hutchinson Cancer Research Center; fSAD, functional small airways disease; PD, parenchymal disease; PRM, parametric response mapping; UM, University of Michigan

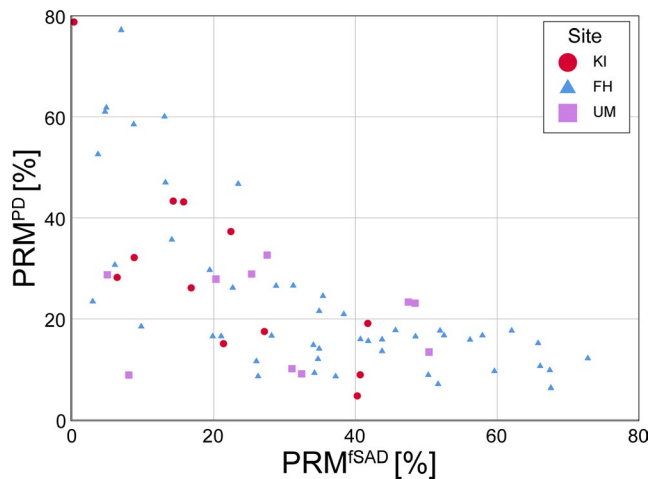


FIGURE 3 Contributions of PRM-derived fSAD and PD in cohort. Presented is a plot of the relative volumes of fSAD (PRM^{fSAD}) and PD (PRM^{PD}) for each of the 72 subjects studied with color-coding for site accrual. A clear trend between the contribution of fSAD and PD is observed. FH, Fred Hutchinson Cancer Research Center; fSAD, functional small airways disease; KI, Karolinska University Hospital; PD, parenchymal disease; PRM, parametric response mapping; UM, University of Michigan

Figure 3 illustrates the relationship between PRM-derived fSAD and PD over the entire study cohort. As expected, most cases had high levels of fSAD (ie, obstructive phenotype). Nevertheless, there were

18 cases, primarily from KI and FH, that were found to have PD levels $> 20\%$ with relatively low levels of fSAD ($< 20\%$), which included 6 cases of mixed ($N = 3$) and restrictive ($N = 3$) physiology by PFT.

The ability of PRM to differentiate the restrictive and obstructive phenotypes was further evaluated by comparing PRM-derived fSAD (obstructive component) and PD (restrictive component) to PFT measurements pooled over all 3 sites. As expected, a drop in FEV1% was found to correspond with an increase in PRM-derived fSAD ($R = -0.236$, $P = .046$). Likewise, for FEV1/FVC, a negative correlation was observed for fSAD ($R = -0.689$, $P < .0001$) (Figure S2), whereas a positive correlation was observed for PD ($R = 0.437$, $P < .0001$). These trends reversed when comparing PRM metrics to FVC% (fSAD: $R = 0.407$, $P < .0001$; PD: $R = -0.486$, $P < .0001$) and TLC (fSAD: $R = 0.623$, $P < .0001$; PD: $R = -0.531$, $P < .0001$). Performing the same analysis over individual site populations found similar correlations between PRM metrics and PFT measurements for KI and FH (Table 2). UM correlations were only observed between fSAD and both FEV1% and FEV1/FVC; of note, all the UM subjects had obstruction.

To determine the contribution of PRM-derived fSAD and PD on these PFT metrics, a multivariable analysis was performed controlling for site and BMI (Table 3). Although in a univariate analysis only fSAD was found to correlate with FEV1% (Table 2), both fSAD and PD were found to be strong parameters for FEV1%. Similar to the univariate analysis, PD and fSAD were strong contributors to statistical models of FVC% and FEV1/FVC, respectively. This is consistent with the negative correlation observed in the univariate analysis. TLC% was only found to correlate with PRM-derived fSAD.

4 | DISCUSSION

In this retrospective analysis, we found that high-resolution chest CT images of patients clinically diagnosed primarily with BOS from 3 centers could be analyzed by PRM for a SAD signature. Variations in the acquisition of CT images across centers accounted for variation in the image quality. Acquisitions with reduced tube current appeared to affect image quality and likely accounted for background ambient noise (Supplemental Section). Nevertheless, variations in acquisition parameters did not diminish the overall ability of PRM to distinguish fSAD from normal and parenchymal disease. Additionally, PRM suggested a signature for restrictive physiology, as the FVC % and TLC % negatively correlated with a parenchymal signature. RLD likely represents a manifestation of chronic GVHD in HCT recipients, analogous to “restrictive allograft syndrome” phenotype of chronic lung allograft dysfunction described in lung transplant recipients.²⁰ In a prospective European cohort, interstitial lung disease represented 21% of the late-onset noninfectious lung complications after allo-HCT, and was associated with a prior diagnosis of chronic GVHD.⁷ Defining the mixed and restrictive PRM phenotypes of lung disease related to chronic GVHD will require additional work with a larger cohort.

Parametric response mapping of paired CT has been investigated extensively as an analytical technique to better phenotype

TABLE 2 Correlations of PRM and PFT for each site

PRM Class	PFT	KI (N = 12)	FH (N = 48)	UM (N = 12)
PRM ^{fSAD}	FEV1 (% predicted)	-0.309, 0.329	-0.208, 0.156	-0.718, 0.002
	FVC (% predicted)	0.634, 0.027	0.438, 0.002	-0.473, 0.121
	FEV1/FVC	-0.778, 0.003	-0.682, <0.0001	-0.705, 0.023 (N = 10)
	TLC (% predicted)	0.780, 0.003	0.682, <0.0001 (N = 47)	0.154, 0.805 (N = 5)
PRM ^{PD}	FEV1 (% predicted)	0.530, 0.076	-0.127, 0.391	-0.387, 0.214
	FVC (% predicted)	-0.725, 0.008	-0.516, <0.0001	-0.194, 0.546
	FEV1/FVC	0.953, <0.0001	0.301, 0.038	0.255, 0.476 (N = 10)
	TLC (% predicted)	-0.885, <0.0001	-0.475, 0.001 (N = 47)	-0.564, 0.322 (N = 5)

Note: Data for each cell represent the *R* value and its *P* value. Those parameters found to be significant are bolded.

Abbreviations: FEV1, forced expiratory volume at 1 s; fSAD, functional small airways disease; FVC, forced vital capacity; PFT, pulmonary function test; PD, parenchymal disease; PRM, parametric response mapping; TLC, total lung capacity. Statistical significance was assessed at a *P* value < .05.

TABLE 3 Multivariable regression

	PRM ^{fSAD}	PRM ^{PD}	BMI	Site (FH)	Site (KI)
FEV1 (% predicted)	-0.449, 0.001	-0.477, 0.001	0.585, 0.062		
FVC (% predicted)		-0.552, <0.0001	0.711, 0.028	11.544, 0.027	
FEV1/FVC	-0.005, <0.0001				0.104, 0.028
TLC (% predicted)	0.404, 0.001			-11.570, 0.057	-13.737, 0.050

Data for each cell represent the parameter coefficient and its *P* value. Those parameters found to be significant are bolded. Statistical significance was assessed at a *P* value < .05. The site University of Michigan (UM) serves as the reference, thus the coefficients for the other sites (FH, KI) represent the intercept relative to UM. For example, FVC% in the FH population is 11.544 higher than in the UM population. For FEV1/FVC, KI is 0.105 higher than UM.

Abbreviations: BMI, body mass index in units of kg/cm²; FEV1, forced expiratory volume at 1 s; FH, Fred Hutchinson Cancer Research Center; fSAD, functional small airways disease; FVC, forced vital capacity; KI, Karolinska University Hospital; PD, parenchymal disease; TLC, total lung capacity.

airway obstruction in COPD.²¹⁻²⁶ Most of these studies are associated with multicenter observational trials such as the COPDGene and SPIROMICS,^{27,28} where imaging protocols are selected to produce image quality consistent across participating sites. This allows consistent results in quantitative CT measures (eg, PRM) across participating centers. The impact of image protocol variability on PRM measurements has been previously evaluated, but only in the context of COPDGene and SPIROMICS CT acquisitions.²⁹ Imaging protocols associated with large multicenter clinical trials do not necessarily reflect local practices of individual hospitals. Nevertheless, our single-center studies have demonstrated PRM as a diagnostic imaging signature in BOS after HCT and lung transplant,¹²⁻¹⁴ which has the potential to aid in the evaluation and the definition of BOS. Given the potential variability of CT imaging protocols at different transplant centers, it was important to investigate the impact of technical and clinical factors on the PRM analysis.

Baseline chest CT image quality was found to vary from site to site and was most pronounced within the expiratory scans. Although acquisition and reconstruction parameters varied between sites (Table S1), this did not appear to affect whole-lung PRM values of fSAD and PD. In fact, results presented in this study suggest that

variations in PRM-derived fSAD and PD are driven more by disease severity and phenotype, as shown by the differences in the PFT parameters of participants at each site. Conventional indices of airways obstruction, including FEV1% and FEV1/FVC, remain independently associated with fSAD signatures when site and BMI are taken into account. Correlations of these measures with pulmonary function measurements have shown PRM-derived fSAD and PD to identify obstructive and restrictive diseases. The observed correlations of fSAD and PD with pulmonary function parameters are consistent with a previously reported study evaluating PRM as a diagnostic biomarker of obstructive and restrictive lung disease in lung transplant recipients with GVHD.¹³ Multivariable analysis of PRM measures, controlling for site of accrual, found that PRM-derived fSAD and PD are independent measures of disease severity and phenotype (Table 3).

The current study has several limitations. First, this is a retrospective study and CT scans were not originally acquired for the purposes of PRM case-control analysis. Due to the wide variability in scanner type, acquisition, and reconstruction, there was an insufficient number of cases to fully evaluate each of the many parameters that affect PRM measurements. This also made it infeasible to acquire controls,

that is, HCT recipients without GVHD scanned using a similar CT protocol, from the 3 centers that participated in this study. The cohort analysis was skewed to FH, which had significantly more patients than the other sites. It is possible that the difference in demographics was responsible for the variations in the PRM signatures. The number of cases was limited for an exploration of restrictive phenotypes. Nonetheless, the purpose of the study was to establish PRM as a valid technique for the diagnosis of clinically recognized BOS, and the study reflects real-world conditions in which heterogeneous phenotypes of BOS exist¹⁶ and different centers will serve populations reflective of that region. The correlation between PRM and PFT measures and PRM-derived fSAD and PD, regardless of site, suggests that PRM will still be diagnostically useful in multiple settings.

For PRM to be broadly applicable and diagnostically accurate, particularly for the diagnosis of early-stage disease, it may be helpful to clarify the protocol requirements for a high-resolution CT imaging and to standardize the acquisition of high-resolution CT images. Based on the results reported in this study, sufficiently high X-ray tube currents, even if incremental scans are required to reduce X-ray exposure, are recommended for minimizing image noise, which would improve PRM measurements. Although recent studies evaluating the utility of PRM as an early detector of BOS are promising, prospective studies in which HRCT are used for screening of patients at risk for pulmonary GVHD disease will help validate the use of PRM for early detection of disease onset and progression.

ACKNOWLEDGMENTS

This work was supported by the US National Institutes of Health research grants R44HL118837, R44HL140894, R01HL139690, R35CA197701, P30CA015704, and P30CA046592.

DISCLOSURE

The authors of this manuscript have conflicts of interest to disclose as described by the *American Journal of Transplantation*. CJG has a financial interest in Imbio, LLC, which has licensed the PRM technology. CH is an employee and stock option holder at Imbio, LLC. The other authors have no conflicts of interest to disclose.

DATA AVAILABILITY STATEMENT

The data that support the findings of this study are available from the corresponding author upon reasonable request.

ORCID

Craig J. Galban  <https://orcid.org/0000-0001-5596-7487>

REFERENCES

- Williams KMCJ, Gladwin MT, Pavletic SZ. Bronchiolitis obliterans after allogeneic hematopoietic stem cell transplantation. *JAMA*. 2009;302(3):306-314.
- Au BK, Au MA, Chien JW. Bronchiolitis obliterans syndrome epidemiology after allogeneic hematopoietic cell transplantation. *Biol Blood Marrow Transplant*. 2011;17(7):1072-1078.
- Chien JW, Duncan S, Williams KM, Pavletic SZ. Bronchiolitis obliterans syndrome after allogeneic hematopoietic stem cell transplantation—an increasingly recognized manifestation of chronic graft-versus-host disease. *Biol Blood Marrow Transplant*. 2010;16(1 Suppl):S106-S114.
- Hildebrandt GC, Fazekas T, Lawitschka A, et al. Diagnosis and treatment of pulmonary chronic GVHD: report from the consensus conference on clinical practice in chronic GVHD. *Bone Marrow Transplant*. 2011. Epub 2011/03/29. doi: bmt201135 [pii].
- Williams KM. How I treat bronchiolitis obliterans syndrome after hematopoietic stem cell transplantation. *Blood*. 2017;129(4):448-455.
- Yanik G, Kitko C. Management of noninfectious lung injury following hematopoietic cell transplantation. *Curr Opin Oncol*. 2013;25(2):187-194.
- Bergeron A, Chevret S, Peffault de Latour R, et al. Noninfectious lung complications after allogeneic haematopoietic stem cell transplantation. *Eur Respir J*. 2018;51(5):1702617.
- Bergeron A, Cheng GS. Bronchiolitis obliterans syndrome and other late pulmonary complications after allogeneic hematopoietic stem cell transplantation. *Clin Chest Med*. 2017;38(4):607-621.
- Cheng GS, Storer B, Chien JW, et al. Lung function trajectory in bronchiolitis obliterans syndrome after allogeneic hematopoietic cell transplant. *Ann Am Thorac Soc*. 2016;13(11):1932-1939.
- Jagasia MH, Greinix HT, Arora M, et al. Diagnosis and staging working group report. *Biol Blood Marrow Transplant*. 2015;21(3):389-401.e1.
- Galban CJ, Han MK, Boes JL, et al. Computed tomography-based biomarker provides unique signature for diagnosis of COPD phenotypes and disease progression. *Nat Med*. 2012;18(11):1711-1715.
- Verleden SE, Vos R, Vandermeulen E, et al. Parametric response mapping of bronchiolitis obliterans syndrome progression after lung transplantation. *Am J Transplant*. 2016;16(11):3262-3269.
- Belloli EA, Degtjar I, Wang X, et al. Parametric response mapping as an imaging biomarker in lung transplant recipients. *Am J Respiratory Critical Care Med*. 2017;195(7):942-952.
- Galban CJ, Boes JL, Bule M, et al. Parametric response mapping as an indicator of bronchiolitis obliterans syndrome after hematopoietic stem cell transplantation. *Biol Blood Marrow Transplant*. 2014;20(10):1592-1598.
- Jagasia MH, Greinix HT, Arora M, et al. National Institutes of Health Consensus Development Project on Criteria for Clinical Trials in Chronic Graft-versus-Host Disease: I. The 2014 Diagnosis and Staging Working Group Report. *Biol Blood Marrow Transplant*. 2015;21(3):389-401.e1.
- Bergeron A, Godet C, Chevret S, et al. Bronchiolitis obliterans syndrome after allogeneic hematopoietic SCT: phenotypes and prognosis. *Bone Marrow Transplant*. 2013;48(6):819-824.
- Stoel BC, Stolk J. Optimization and standardization of lung densitometry in the assessment of pulmonary emphysema. *Invest Radiol*. 2004;39(11):681-688.
- Shamonin DP, Bron EE, Lelieveldt BP, Smits M, Klein S, Staring M. Alzheimer's Disease Neuroimaging I. Fast parallel image registration on CPU and GPU for diagnostic classification of Alzheimer's disease. *Frontiers in Neuroinformatics*. 2013;7. <https://doi.org/10.3389/fninf.2013.00050>.
- Klein S, Staring M, Murphy K, Viergever MA, Pluim J. elastix: a toolbox for intensity-based medical image registration. *IEEE Trans Med Imaging*. 2010;29(1):196-205.
- Shah RJ, Diamond JM. Update in chronic lung allograft dysfunction. *Clinics Chest Med*. 2017;38(4):677-692
- Vasilescu DM, Martinez FJ, Marchetti N, et al. Non-invasive imaging biomarker identifies small airway damage in severe COPD. *Am J Respir Crit Care Med*. 2019. <https://doi.org/10.1164/rccm.201811-2083OC>.
- Martinez CH, Diaz AA, Meldrum C, et al. Age and small airway imaging abnormalities in subjects with and without airflow obstruction in SPIROMICS. *Am J Respiratory Critical Care Med*. 2017;195(4):464-472.

23. Labaki WW, Gu T, Murray S, et al. Voxel-wise longitudinal parametric response mapping analysis of chest computed tomography in smokers. *Academic Radiol.* 2019;26(2):217-223.
24. Han MK, Tayob N, Murray S, et al. Association between emphysema and chronic obstructive pulmonary disease outcomes in the COPDGene and SPIROMICS cohorts: a post hoc analysis of two clinical trials. *Am J Respir Crit Care Med.* 2018;198(2):265-267.
25. Boes JL, Hoff BA, Bule M, et al. Parametric response mapping monitors temporal changes on lung CT scans in the subpopulations and intermediate outcome measures in COPD Study (SPIROMICS). *Acad Radiol.* 2015;22(2):186-194.
26. Bhatt SP, Soler X, Wang X, et al. Association between functional small airway disease and FEV1 decline in chronic obstructive pulmonary disease. *Am J Respir Crit Care Med.* 2016;194(2):178-184.
27. Regan EA, Hokanson JE, Murphy JR, et al. Genetic Epidemiology of COPD (COPDGene) study design. *J Chron Obstruct Pulmon Dis.* 2011;7(1):32-43
28. Sieren JP, Newell JD, Barr R, et al. SPIROMICS protocol for multicenter quantitative computed tomography to phenotype the lungs. *Am J Respir Crit Care Med.* 2016;194(7):794-806
29. Boes JL, Bule M, Hoff BA, et al. The impact of sources of variability on parametric response mapping of lung CT scans. *Tomography.* 2015;1(1):69-77.

SUPPORTING INFORMATION

Additional supporting information may be found online in the Supporting Information section.

How to cite this article: Cheng G-S, Selwa KE, Hatt C, et al. Multicenter evaluation of parametric response mapping as an indicator of bronchiolitis obliterans syndrome after hematopoietic stem cell transplantation. *Am J Transplant.* 2020;20:2198-2205. <https://doi.org/10.1111/ajt.15814>